energies

MDPI

Article

Chemistry of Reservoir Fluids in the Aspect of CO_2 Injection for Selected Oil Reservoirs in Poland

Ewa Knapik * and Katarzyna Chruszcz-Lipska

Drilling, Oil and Gas Faculty, AGH University of Science and Technology, al. Mickiewicza 30, 30-059 Krakow, Poland; lipska@agh.edu.pl

* Correspondence: eknapik@agh.edu.pl; Tel.: +48-12-617-2208

Received: 6 October 2020; Accepted: 2 December 2020; Published: 6 December 2020

Abstract: Worldwide experiences related to geological CO_2 storage show that the process of the injection of carbon dioxide into depleted oil reservoirs (CCS-EOR, Carbon Capture and Storage—Enhanced Oil Recovery) is highly profitable. The injection of CO_2 will allow an increasing recovery factor (thus increasing CCS process profitability) and revitalize mature reservoirs, which may lead to oil spills due to pressure buildups. In Poland, such a solution has not yet been implemented in the industry. This work provides additional data for analysis of the possibility of the CCS-EOR method's implementation for three potential clusters of Polish oil reservoirs located at a short distance one from another. The aim of the work was to examine the properties of reservoir fluids for these selected oil reservoirs in order to assure a better understanding of the physicochemical phenomena that accompany the gas injection process. The chemical composition of oils was determined by gas chromatography. All tested oils represent a medium black oil type with the density ranging from 795 to 843 g/L and the viscosity at 313 K, varying from 1.95 to 5.04 mm/s. The content of heavier components C25+ is up to 17 wt. %. CO_2–oil MMP (Minimum Miscibility Pressure) was calculated in a CHEMCAD simulator using the Soave–Redlich–Kwong equation of state (SRK EoS). The oil composition was defined as a mixture of n-alkanes. Relatively low MMP values (*ca*. 8.3 MPa for all tested oils at 313 K) indicate a high potential of the EOR method, and make this geological CO_2 storage form more attractive to the industry. For reservoir brines, the content of the main ions was experimentally measured and CO_2 solubility under reservoir conditions was calculated. The reservoir brines showed a significant variation in properties with total dissolved solids contents varying from 17.5 to 378 g/L. CO_2 solubility in brines depends on reservoir conditions and brine chemistry. The highest calculated CO_2 solubility is 1.79 mol/kg, which suggest possible CO_2 storage in aquifers.

Keywords: CO_2 injection; EOR; MMP (Minimum Miscibility Pressure) calculation; CHEMCAD

1. Introduction

The EU climate policy assumed that the emission of CO_2 will be reduced by 40% by 2030 compared to 1990 [1]. In September 2020, the European Commission proposed to raise the 2030 greenhouse gas emission reduction target to at least 55% to reach 2050 climate neutrality goal [2]. In order to maintain the competitive position and improve costs related to adaptation to low-emission management, it is necessary to develop CCS technology. Technical problems related to the separation of CO_2 are well-known and in most cases well-managed [3,4]. A substantial advancement in terms of construction and material solutions allows separating CO_2 in any scale and controlling the product parameters with high precision. A high level of full feasibility is confirmed by numerous industrial systems operating for the within the food or chemical industry [5,6]. Similarly, a number of pilot systems intended for heat- and power-generating plants show a high level of CO_2 recovery from waste gases, and a high purity of the final product. Yet, it is an economic issues that poses the most serious

obstacle in the process of capturing CO_2 widely [7]. In the industry, particularly the European one, there is no demand for large amounts of CO_2. It is used in refrigerating engineering, the brewing industry, the food industry, and as a supercritical solvent, but it is a low-tonnage application which is insufficient when compared to the volume of CO_2 streams emitted by heat- and power-generating plants. Considering large-scale technologies of CO_2 use, we can distinguish the following: enhanced oil recovery, enhanced coal bed methane production, advanced geothermal systems, algae cultivation, CO_2 mineralization, concrete hardening, and the production of fuels, polymers and valuable chemical materials [8–10]. So far, only resource recovery applications, including enhanced oil recovery (EOR), enhanced gas recovery (EGR), fracturing, enhanced coal bed methane production (ECBM) and oil shale recovery, have been implemented in the industry, and bring positive economic effects. It is estimated that globally, CO_2-enhanced oil recovery has the technical potential to use up to 16 to 22 billion t CO_2 by 2050, with a relatively high-net benefit (USD ~100/t CO_2) [11].

An excellent example of the beneficial use of CO_2 is its injection into shale oil reservoirs for enhanced oil recovery. Experimental core flooding tests performed by Kurz et al. [12] showed that supercritical CO_2 can extract 12~65% of hydrocarbons from the organic-rich Bakken shales within 24 h. Gamadi et al. [13] studied the CO_2 huff-n-puff method on Mancos and Eagle Ford cores, achieving up to 85% oil recovery. Song and Yang [14] performed CO_2 huff-n-puff experiments under different operation pressures ranging from 7 to 14 MPa using the Bakken cores. In the immiscible scenario at a low injection pressure, only 42.8% of oil was recovered, while above the MMP the total oil recovery reached 63%. Some reported field pilots in the Eagle Ford formation showed a great performance of gas injection with a 30–70% improved oil production [15]. However, some field trials in Bakken formation were not successful due to the gas early breakthrough. The key parameter for successful CCS-EOR is a detailed reservoir characterization. Jia et al. [16] comprehensively reviewed the feasibility and advances of CO_2 injection in shale reservoirs in terms of injection scheme, oil recovery mechanisms, role of molecular diffusion, nanopore effect on the phase behavior and adsorption effect on carbon storage. The authors summarized the available experimental studies and pilot tests, giving a holistic guideline about CO_2 injection techniques for unconventional reservoirs.

Poland has significant prospects for the implementation of CCS [17]. It also seems that Poland has a large potential with regard to the implementation of CCS-EOR methods. In 2017, CO_2 emission was estimated at the level of about 336.56 million tonnes, as reported to the EU under the EU Emissions Trading Scheme, and the main source of CO_2 emission was fuel consumption (92.5%) [18]. Four Polish power plants (Bełchatów, Kozienice, Turów and Rybnik) belong to the category of the top 30 most CO_2-polluting thermal power plants in the EU [19]. When it comes to CO_2 capturing, two pilot plants have been constructed: an amine absorption unit in Łaziska power plant and a pressure swing absorption unit connected to the gas pass of the world's largest fluidized-bed boiler (460 MW unit) in the Łagisz power plant [20,21]. As far as capturing technology is concerned, there are no legal and technological obstacles for this type of systems. The problem is the issue related to geological CO_2 storage because the storage location (distance from the CO_2 emitter, population density) determines the profitability of the entire project. So far, two geological storage projects have been carried out in Poland. The RECOPOL project was an EC-funded research project to investigate the technical and economic feasibility of storing CO_2 permanently in subsurface coal seams in the Upper Silesian Coal Basin [22]. Another example of a domestic project is Europe's oldest acid gas reinjection (CO_2 and H_2S) system, operating since 1995 in the Borzęcin gas reservoir [23]. Over the last 20 years of exploitation, nearly 700 t of H_2S and 3400 t of CO_2 have been injected. Both projects have proved to be fully capable of storing, yet have not brought any economic success. American and Canadian experience (the Weyburn and Midale oil fields in Canada, since 2000, and more than 30 oil fields in West Texas, USA) demonstrates that CO_2 injection pays off solely if accompanied by the production of natural gas or oil [24,25].

In Poland, no EOR-CO_2 project has been carried out even though there are a lot of depleted oil reservoirs. Particular reservoirs located in the Polish Lowland and in the area of the Carpathian Foredeep are known to have inconsiderable storage capacities. The literature data have presented the CO_2 storage capacities of particular hydrocarbon reservoirs in Poland [26]. In general, the storage capacity calculated for Polish hydrocarbon fields, using an assumption of a 1:1 volumetric replacement of hydrocarbons with supercritical CO_2, is 764.32 Mt of CO_2. Tarkowski et al. [26] calculated storage capacity only for a few oil reservoirs, including Jastrząbka (0.42 Mt), Węglówka (1.87 Mt) and Kamień Pomorski (3.93 Mt). Deeper knowledge about the possibility of CO_2 storage in other oil reservoirs is still necessary. According to Wojnarowski [27], more than 30 oil reservoirs may be considered for CCS purposes.

Thus, the aim of this work was to predict CO_2 behavior in the presence of reservoir fluids from five selected formations identified by Mikołajczak et al. [28] as suitable for CO_2 storage. During the selection of these reservoirs, only geological aspects were considered (reservoir depth, porosity, oil recovery) to ensure the high storage safety and capacity. The CO_2 injection may be realized as miscible or immiscible flooding, which affects the displacement efficiency. During the immiscible injection, an early gas breakthrough occurs, which leads to lower oil recovery. In this work an assessment of whether miscibility is possible is performed to determine the feasibility of such EOR projects in Poland.

2. Materials and Methods

2.1. Reservoir Fluids

Mikołajczak et al. [28] identified only 4 possible clusters of reservoirs (a set of at least 2 reservoirs is considered as a cluster) suitable for CCS-EOR in Poland. Such clusters have higher CO_2 storage capacities than individual formations. In southern Poland two possible clusters have been found. The samples of reservoir fluids from reservoirs located in the southwest area of the Subcarpathian Province are described as SP1 and SP2. The second cluster is situated in the Lesser Poland Province and samples are described as LP1 and LP2. The samples from the largest oil reservoir located in the Polish Lowland are described as PL1. Oil samples were taken from multiple-well stock tanks. The oil was initially saturated with gas at the separator (tank) pressure so all samples were degassed before further experiments at room conditions. The obtained field crude oil samples were cleaned by using a centrifuge (Chirana, Slovakia) to remove any sand and brine. All formation water samples were either collected from the production string at the pumpjack or from a separator. Sampling was processed in a manner similar to that of Kharaka et al. [29].

2.2. Analytical Methods

All basic properties of the oil samples were measured according to ASTM standard methods. The ractional composition of particular fluids was identified by the GC-FID (Gas Chromatography with Flame-Ionization Detection) method. Whole oils were analyzed on a Hewlett/Packard Model 5890 (HP5890) gas chromatograph fitted with 30 m × 0.32 mm × 0.25 µm fused silica column coated with a nonpolar stationary phase (RTX-1). The oven was heated from 313 K to 603 K at the rate of 10 K/min for the final isothermal period of 25 min. The carrier gas was helium at a flow rate of 2.3 mL/min. The data were processed using the ChemStation Rev.A.10.01 software.

All physiochemical analysis of formation water were performed in accordance with the methods presented in the Standards Methods for the Examination of Water and Wastewater [30]. Conductivity and pH were measured using a portable CC-315 Elmetron conductivity meter in the field. Due to high salinity, all samples were diluted by 10 or 100 times with deionized water. For cations analysis, samples were filtered and acidified (HNO_3, ACS grade) to pH < 2. Cations contents were analyzed via atomic absorption spectroscopy (Perkin Elmer AAnalyst 100). Total dissolved solids (TDS) were measured after evaporation at 453 K.

2.3. Phase Equilibrium Calculations

2.3.1. CO_2–Oil MMP Calculations

For the purposes of MMP calculating, the CHEMCAD 7.1.8 software version by Chemstations Inc. was used. CHEMCAD is a popular simulator in process engineering and provides a wide range of components and a vast array of equations of state. The oils were defined as mixtures of *n*-alkanes C6–C25. Each pseudo-fraction was represented as a corresponding *n*-alkane. The components heavier than *n*-pentacosane were summed up and added to the C25 pseudo-fraction. For each of the oils a separate simulation was performed. Additionally, to verify the calculation accuracy of the MMP for CO_2-pure *n*-decane was calculated and the results were compared with experimental values.

Since CHEMCAD is not a typical reservoir simulator, the FLASH tool was applied to simulate fluid miscibility. In oil field applications the FLASH designates a pressure vessel used for separating reservoir fluids into gas, oil and water, with three fluids being discharged separately. In this work at the top of the separator a gaseous phase is released (stream 4, Figure 1), whereas at the bottom of the separator oil flows out (stream 5). As feed streams, pure gaseous CO_2 (stream 1) and simulated crude oil (stream 3) were used. At this stream configuration the calculated MMP value corresponds to the stock tank oil (dead oil). In the real reservoir condition, crude oil has dissolved natural gas in it. To recreate the effect of dissolved gas on the MMP value the additional stream containing 95 mole % methane and 5 mole % ethane (stream 2) was introduced to the vessel. The mass ratio of natural gas and crude oil was changed from 0.01:1 to 0.1:1 to check if the miscibility between CO_2 and live oil is dependent on the amount of C_1–C_2 components in the system. In these calculations the oil:CO_2 ratio was constant and equal to 1:10. When the MMP value was calculated for the dead oil, the flow ratio of this natural gas stream was equal to zero.

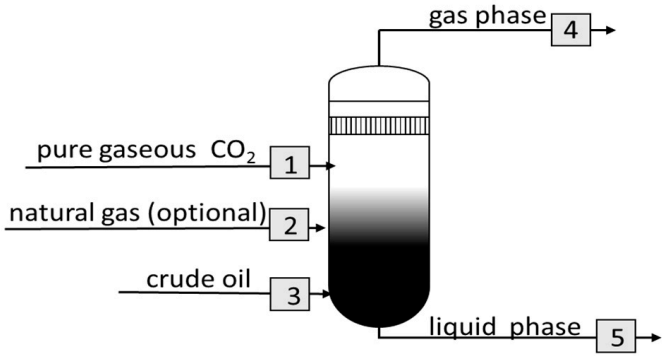

Figure 1. Streams configuration for MMP calculation using CHEMCAD's FLASH tool.

A two-phase flash module simulates a rigorous vapor–liquid calculation. The phase equilibrium was calculated using the Soave–Redlich–Kwong equation of state (SRK EoS). The general form of SRK EoS is described elsewhere [31,32]. Karim et al. [33] provided an instruction for building a simulation scheme in both CHEMCAD and HYSYS simulators. In this work a detailed flow chart of the iterative algorithm for determining the vapor–liquid phase equilibrium in a multicomponent system given by Akberov [34] was followed. The required input data for the EoS modeling (critical pressure, critical temperature and Pitzer acentric factor) for each component were incorporated from CHEMCAD's library. The standard van der Waals mixing rules were used. No "matching" or "tuning" to experimental phase equilibrium data was applied.

The CO_2–oil miscibility can be achieved at first or multiple contacts. The first contact MMP is the lowest pressure at which the reservoir oil and injected CO_2 form a single phase upon their initial contact at any mass/volume ratio [35]. Miscible CO_2 flooding is usually more complex and there is a transition zone wherein a continuous mass transfer between phases occurs. This multi-contact miscibility can be achieved by condensation and/or vaporization mechanisms. The multiple contact

MMP value is lower than the first contact MMP. In this work the FLASH tool corresponds to a single cell where CO_2 and oil are contacted at different ratios, thus the calculated value of MMP by this technique can be considered as FC MMP (First Contact Minimum Miscibility Pressure). During the so-called "sensitivity study" the initial CO_2:oil ratio was changed from 1:1 to 10:1. The lowest pressure at which no gaseous CO_2 stream was recorded after separation is here reported as FC MMP.

2.3.2. Modeling of CO_2 and CH_4 Solubility in Brines

CO_2 solubility in brines was calculated in a similar way to the MMP value. The streams of gaseous CO_2 and brine were introduced into the separator vessel at a constant mass ratio equal to 1:1 and the CO_2 fraction in the aqueous phase at given conditions was recorded. This work assumes non-reactive conditions (i.e., no geochemical reactions take place concurrent with CO_2 injection, flow and dissolution). The solubility of CO_2 in brines was calculated in a wide temperature–pressure–ionic strength range from 299 to 392 K, from 6.4 to 55.65 MPa and from 17 to 379 g/L TDS content. The widely used geochemical simulators [36] PHRQPITZ, PHREEQC, TEQUIL, EQL/EVP and EQ3/6 are based on Pitzer's equation; thus this option was also chosen in CHEMCAD. The Pitzer equation describes the thermodynamic behavior of electrolyte solutions and allows one to calculate osmotic and activity coefficients [37]. The complex composition of brines have been simplified to keep the proportions of the dominant ions Na^+, K^+, Ca^{2+}, Mg^{2+}, Cl^-, CO_3^{2-}, HCO_3^- and SO_4^{2-}. CH_4 solubility in brines was calculated in a similar manner.

3. Results and Discussions

3.1. Crude Oils Characterization

For the purposes of CCS-EOR, light paraffinic crude oil with a low content of asphaltenes is highly useful. At favorable conditions, CO_2 mixes with the crude oil and the oil displacement is called miscible. The basic physiochemical properties of the tested oils have been specified in Table 1.

Table 1. Crude oils properties.

Parameter/Field	Method	PL1	SP1	SP2	LP1	LP2
Density (g/L)	ASTM D287	795	843	837	837	827
Viscosity at 313 K (mm^2/s)	ASTM D445	1.95	5.04	4.01	4.32	2.01
Acid number (mg KOH/g)	ASTM D974	0.356	0.172	0.198	0.427	0.246
Asphaltene content (wt. %)	ASTM D6560	0.953	0.749	1.035	1.819	0.997
Conradson carbon residue (wt. %)	ASTM D189	0.544	2.566	2.195	0.901	0.533

Basically, the oils do not differ substantially in terms of their properties; they belong to medium black oils. However, some differences in terms of acid number (from 0.172 to 0.427 mg KOH/g), Conradson residue (0.533–2.566 wt. %) and the content of C25+ (from 7.34 to 16.92 wt. %) were reported. A gas chromatogram of whole oil for the sample from the LP2 oil field is shown in Figure 2. The chromatograms of the other four oil samples are shown in Appendix A.

The oils have a comprehensive range of light and medium components. The values of the Conradson carbon residue are low for all samples, so there are only small losses of analytes observed during GC measurements, as resins and asphaltenes are not detectable by capillary gas chromatography. The chromatographic analysis reveals slight differences in the boiling-point distribution of the chromatographable hydrocarbons. The LP2 oil includes a broad suite of n-alkanes, which is conspicuous in Figure 2, where the n-alkane peaks are significantly larger than others. LP2 oil is relatively light; the content of gasoline compounds C6–C12 is up to 54.6 wt. %. The chromatogram for LP1 oil shown in Figure A1 in the Appendix A is similar to that of Figure 2, but contains a greater proportion of diesel fuel compounds (e.g., C13–C20). Figure A2 shows the chromatogram of another paraffinic-rich oil PL1 enriched in C6–C12 hydrocarbons in the gasoline range (more than 50 wt. %), and a smaller

proportion of residual range hydrocarbons. The chromatogram of oil from the SP2 oil field has a bimodal distribution of n-alkanes that peak at about *n*-C12 and *n*-C18 (Figure A3). SP1 oil contains slightly higher amounts of heavier compounds than the others (Figure A4). The GC/FID chromatograms of these oils demonstrate that they contain varying amounts of a broad-cut fuel range (~C6–C25), hence their usability in conversion into useful products.

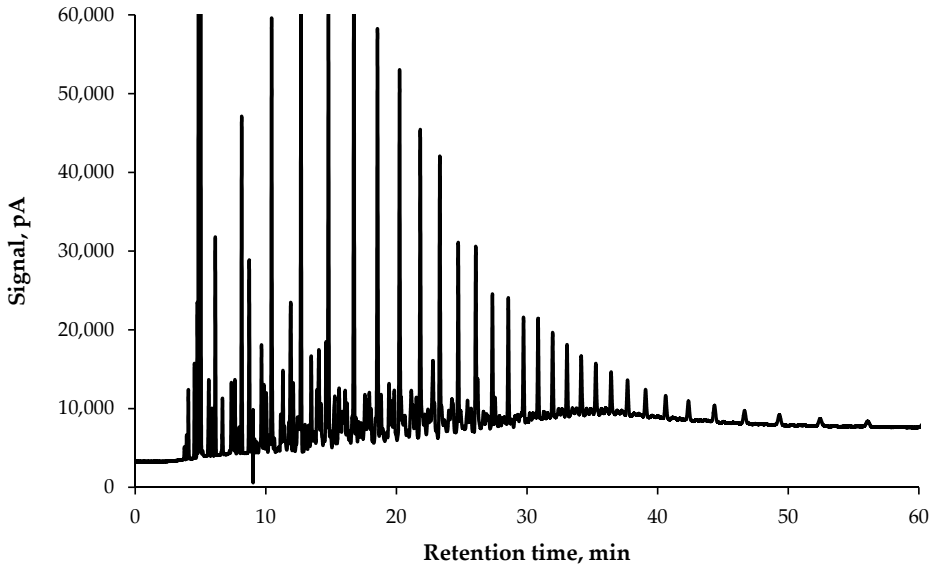

Figure 2. Whole LP2 oil gas chromatogram.

Based on the GC results, the composition of each of the oils was quantified using the pseudo-fractions approach. The components between two neighboring normal alkanes are here grouped together and reported as a pseudo-fraction, equal to that of a higher normal alkane. For example, the hydrocarbon fraction C10 is made up of all component peaks appearing after *n*-nonane (excluded) and *n*-decane (included). The theoretical contents of the pseudo-fractions in oils are presented in Table 2. The physiochemical properties of each pseudo-fraction are unknown, so for calculation purposes in the CHEMCAD simulator these pseudo-fractions were defined as pure corresponding *n*-alkanes.

Table 2. The calculated composition of oils in wt. % used for MMP calculations.

Component/Field	PL1	SP1	SP2	LP1	LP2
C6	7.63	4.51	6.22	3.75	4.23
C7	9.88	5.43	7.53	4.4	6.98
C8	11.44	5.06	7.56	6.31	8.53
C9	10.15	5.88	7.36	7.30	9.32
C10	7.12	4.32	5.30	6.73	9.35
C11	5.80	3.72	4.47	7.18	8.19
C12	6.14	5.15	6.11	7.57	8.02
C13	5.06	4.97	5.50	6.70	7.25
C14	5.31	5.27	5.48	7.42	6.74
C15	3.93	4.30	4.26	6.32	5.37
C16	3.36	4.53	4.36	4.93	3.54
C17	3.31	5.45	4.99	4.97	3.54
C18	3.55	3.91	3.41	3.39	2.35
C19	2.48	4.00	2.81	3.37	2.15
C20	1.93	4.08	3.03	2.84	1.57
C21	1.34	3.39	3.24	2.28	1.52
C22	1.50	3.23	2.68	2.31	1.59
C23	1.31	3.02	2.56	2.33	1.30
C24	1.34	2.86	2.40	1.94	1.12
C25	7.42	16.92	10.73	7.96	7.34

3.2. CO_2–Oil MMP Calculations

To prove the correctness of the suggested method of MMP calculation, the MMP was determined for the CO_2–*n*-decane system and compared to the literature's data. For calculation purposes, the mass flow ratio of CO_2 (stream 1) and n-decane (stream 3) was changed from 1:1 to 10:1. Figure 3a shows the mass flow rate of gaseous stream 4 after phase separation under pressure ranging from 7 to 8 MPa. When the flow rate of stream 4 is equal to zero, it is assumed that the CO_2 is fully soluble/miscible with *n*-decane (the MMP is achieved), and only one liquid phase exists. The CO_2:*n*-decane mass ratio insignificantly affects the calculated MMP value.

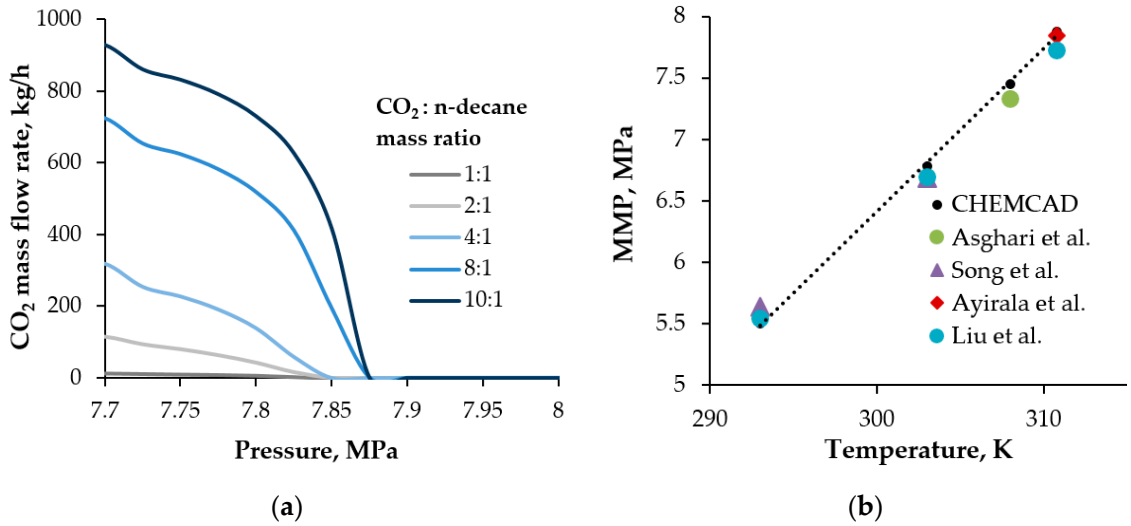

Figure 3. (**a**) Mass flow rate of the gaseous CO_2 stream contacted with *n*-decane at different mass ratios in conditions close to MMP at 310.95 K, (**b**) comparison between experimental MMP values reported by [38–41] and results calculated by SRK EoS in the CHEMCAD simulator.

The literature's data show that the value of MMP for the CO_2–*n*-decane system at the temperature of 310.95 K determined using different approaches differs slightly. Elsharkawy et al. [42] has reported a slim-tube MMP of 8.2–8.6 MPa and an RBA (rising bubble apparatus) MMP of 8.8 MPa. Ayirala et al. [38] measured a VIT (vanishing interfacial tension) MMP of 7.8 MPa. Song et al. [40] estimated MMPs for the CO_2–*n*-decane system at various temperatures (5.637, 6.682, and 7.791 MPa for 293, 303, and 310.95 K, respectively) using the MRI (magnetic resonance imaging) technique. The criteria of determining MMP in particular methods vary, and are frequently based on visual observation, thus the reported values are slightly different. Figure 3b shows the comparison between MMP values predicted by SRK EoS and experimental results reported by other researchers. The calculated results demonstrate a good agreement with the experimental values, which confirms the accuracy of the proposed calculation method. The SRK EoS is a thermodynamic model suitable for predictions of the CO_2–n-alkanes' phase behavior.

Czarnota et al. [43] measured the value of MMP for the CO_2–LP2 oil system at different temperatures. The registered values of MMP varied from 6.3 MPa at 295 K to 12.3 MPa at 333 K. The authors did not provide the amounts of fluids used in these experiments, but since in the simulator it is necessary to define the stream volume/mass, it was checked if the mass ratio of the components influences the calculated values. In this work the mass ratio CO_2:LP2 oil was changed from 1:1 to 10:1, and for all simulations no gas phase above the reported MMP values was observed (Figure 4a).

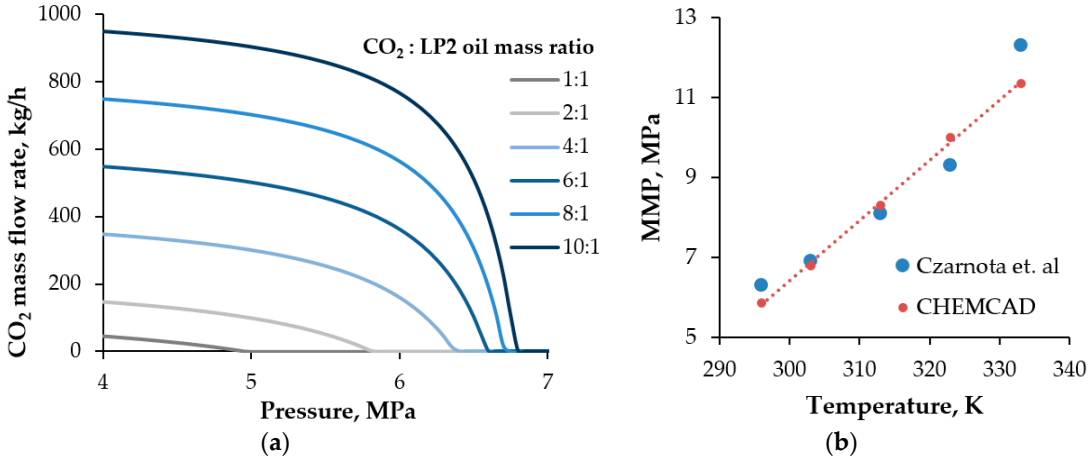

Figure 4. (**a**) MMP at different mass ratio CO_2:LP2 oil at 303 K, (**b**) comparison between measured [43] and predicted values of MMP for LP2 oil.

In this work the same LP2 oil was tested that Czarnota et al. [43] used in their study, so the reported experimental values can be used for the fluid model's validation. In this study the oil composition is simplified to a mixture of n-alkanes without any further tuning. The comparison between experimental MMP values for LP2 oil and the predicted values (Figure 4b) confirms the accuracy of this simplified approach. The calculation relative error changes from 1.45 to 7.72% at higher temperatures. For comparison, Zhang et al. [44] used for the MMP calculation a tuned Peng–Robinson EoS, taking into account the PVT properties of oil, and the error ranged from 1.9 to 10.7%. The mass proportion between oil and CO_2 has a greater influence on their mutual miscibility than in the CO_2/*n*-decane system. As shown in Figure 4a, when equal amounts of CO_2 and oil are used, the miscibility occurs at 6.0 MPa, and this value shifts to 8.3 MPa at higher CO_2 contents. In reservoir conditions it is possible that in the porous space CO_2 prevails (near-wellbore zone for CO_2 injection well), but there are also zones with high oil saturation. Figure 4a shows that the smallest amount of CO_2 (100 kg of CO_2/100 kg of oil) dissolves in oil at relatively low pressures. The increase in mass ratio above 6:1 does not influence the miscibility pressure, and with regard to all mass ratios has a fixed value. The calculations obtained by using the SRK equation for the CO_2–LP2 system fit well with the experimental observations. Thus, the above-described method was used to determine MMP for all the crude oils studied in this work, and the results of the simulation were gathered in Table 3. MMP was calculated at 313 K for comparison purposes and at individual reservoir temperatures. In Figures A5–A9 in the Appendix A, the graphical determination of the MMP for each of the oils is shown. The MMP values are similar for all oils; at 313 K the MMP is ca. 8.3 MPa. The MMPs at reservoir temperatures are lower than the initial reservoir pressures, which guarantees that the injected CO_2 does not breach reservoir integrity.

Table 3. Reservoir properties of oil fields at initial conditions [45] and the calculated MMP values.

Parameter/Field	PL1	SP1	SP2	LP1	LP2
Initial reservoir pressure (MPa)	55.65	24.4	21.15	6.40	8.84
Reservoir temperature (K)	392	338	325	299	307
Oil recovery factor, R_o (-)	0.088	0.471	0.204	0.347	0.544
Calculated MMP at 313 K (MPa)	8.28	8.45	8.33	8.38	8.25
Calculated MMP at reservoir temperature (MPa)	18.10	12.93	10.55	6.29	7.38

Figure 5a shows the effect of dissolved gas on the MMP value for the CO_2–SP2 oil system. The amount of gas is given as the gas/oil ratio (GOR) which is the ratio of the volume of released natural gas to the volume of oil under standard conditions. The MMP increases with an increasing GOR value. Similar effects were reported by Zhang et al. [44] for two light oils from Saskatchewan (Canada). The authors found that the CO_2 MMP of the Weyburn reservoir fluid was 11.7 MPa at 332 K. When impure CO_2 containing up to 9.9 mole % CH_4 or 3.1 mole % N_2 + 2.8 mole % CH_4 was used, the MMP value was 16.0 and 14.5 MPa, respectively. However, when the impurities content in the CO_2 stream was increased to 5.1 mole % N_2 + 5.1 mole % CH_4, the MMP rose to 20.5 MPa. The effect of propane presence in the system gives an opposite effect. The pure CO_2 MMP for the Steelman stock tank oil was equal to 11.8 MPa at 334 K. This value was reduced by 45% when the CO_2 contained 37 mole % of propane. When live oil from the Steelman reservoir well with GOR equal to 131 m^3/m^3 was used, the pure CO_2 MMP increased to 16.7 MPa [46]. The oils from the tested fields had a gravity of 879 and 834 g/L, and asphaltene contents of 6.7% and 1% by weight, respectively. Despite these differences, the MPP for both oils had a similar value at almost the same temperature. Alston et al. [47] developed an empirical correlation that accounts for the effects of solution gas (live oil systems) and the effects of impure CO_2 on MMP.

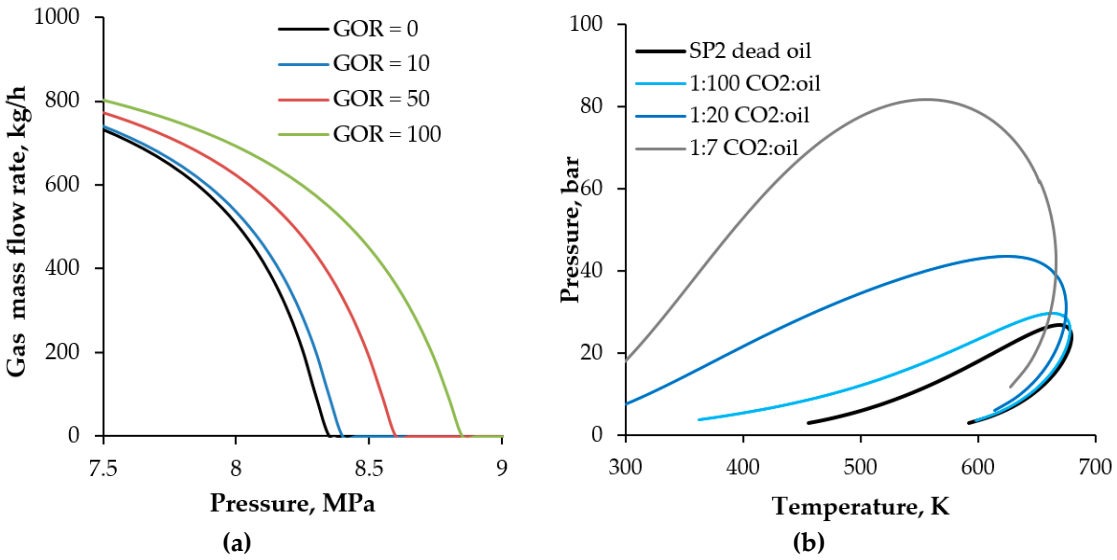

Figure 5. (**a**) Impact of natural gas on the MMP of the CO_2:LP2 oil system at 313 K, (**b**) phase behavior of the CO_2–SP2 oil system.

The amount of dissolved CO_2 influences greatly the phase behaviour of hydrocarbon fluids. Figure 5b shows the phase diagram of SP2 oil with different contents of dissolved CO_2. The knowledge of phase transformations is vital to understand the interaction between the produced fluid and individual elements of the production system, including the reservoir, tubing, separators, pipelines, etc. The basic SP2 oil is dead oil, wherein all dissolved gases and volatile components are released due to the pressure drop during the exploitation. This type of oil is difficult to produce from the reservoir. CO_2 injection helps in increasing fluid mobility, thus, the more CO_2 dissolved, the easier it will be to initiate and sustain oil flow.

Determination of the MMP value is a key step in a well-designed CO_2 injection project. The miscible CO_2 flooding is a complex phenomenon wherein different reservoir aspects should be considered. With increasing reservoir temperature, the MMP increases significantly; for PL1 oil at the highest reservoir temperature of 392 K the miscibility is achieved at pressures above 18 MPa. The MMP values specified in Table 3 are the first contact MMPs, but it can be expected that the miscibility between oil and CO_2 will be developed under lower pressures after multiple contacts. In conventional oil reservoirs, the oil recovery mechanism includes convective flow, gravity drainage and a diffusion process [16].

In tight formations the mutual miscibility strongly depends on molecular diffusion, as proven by Jia et al. [48]. Diffusion in the porous media is affected by tortuosity and porosity, hence for more realistic simulations the CO_2 diffusion coefficient in the oil-saturated porous media should be measured, rather than that in the bulk phase [49,50]. The porous structure of the rock matrix plays the major role in the mass transfer, and can affect the MMP. Wang et al. [51] calculated the CO_2 MMP of Bakken oil taking into account the pore size. Their results show that the MMP is independent of pore diameter in pores of sizes larger than 10 nm. For example, if the pore width decreases from 10 to 3 nm, the MMP decreases by 23.5%. The low values of MMP obtained in this study are an important prerequisite for possible CO_2 injection into Polish oil reservoirs. However, to upscale the phase behavior of oil and CO_2 from the pore scale to the field scale, more research with real rock cores is needed.

3.3. CO_2 and CH_4 Solubility in Brines

High brine mineralization suggests a lack of connection between the reservoir and underground water, and a lack of infiltration of rainwater. In the United States, by regulation, in order for a geological reservoir to be considered suitable for carbon storage, it must contain formation brine with total dissolved solids (TDS) > 10,000 ppm [52]. The brine composition is vital if we consider CO_2 storage in aquifers due to the fact that CO_2 is likely to dissolve in water and mineral precipitation may occur. Table 4 shows the basic physicochemical properties of the appropriate brines.

Table 4. Physicochemical properties of brines from selected oil fields in Poland.

Parameter	PL1	LP1	LP2	SP1	SP2
pH	6.2	7.6	8.6	8.0	8.9
Conductivity (mS/cm)	1080	127	52.5	31	29
Total suspended solids (g/L)	0.056	0.188	0.033	0.363	0.215
Total dissolved solids (g/L)	378.900	50.105	17.515	20.780	19.580
Cl^- (g/L)	174.410	26.394	8.644	10.630	9.794
$SO_4{}^{2-}$ (g/L)	3.980	2.405	1.550	0.316	0.322
$CO_3{}^{2-}$ (g/L)	0.000	0.000	0.000	0.002	0.350
$HCO_3{}^-$ (g/L)	0.000	0.000	0.000	0.390	2.385
Na^+ (g/L)	75.200	13.820	5.304	7.379	7.866
K^+ (g/L)	4.527	0.483	0.148	0.048	0.063
Ca^{2+} (g/L)	29.852	1.403	0.532	0.032	0.060
Mg^{2+} (g/L)	2.553	1.386	0.255	0.021	0.013

The literature presents numerous results about changeable permeability and mechanical properties as a result of CO_2–fluid–mineral interactions [53–55]. Adamczyk et al. [56] reported in detail the formation and dissociation of carbonic acid according to the following scheme:

$$CO_{2(sc)} + 3H_2O \leftrightarrow H_2O + CO_{2(aq)} \quad (1)$$

$$H_2O + CO_{2(aq)} \leftrightarrow H_2CO_3 \quad (2)$$

$$H_2CO_3 \leftrightarrow HCO_3{}^- + H^+ \quad (3)$$

$$HCO_3{}^- \leftrightarrow CO_3{}^{2-} + H^+ \quad (4)$$

According to Gaus et al.'s [57] studies, the corrosive nature of dissolved CO_2 is limited in the presence of carbonate rocks which, serve as a buffer according to the following reaction:

$$CaCO_3 + H^+ \leftrightarrow Ca^{2+} + HCO_3{}^- \quad (5)$$

Furthermore, studies conducted by Rimmelé et al. [58] for Lavoux limestone and Adamswiller sandstone and Hangx et al. [59] for Zechstein anhydrite caprock showed no significant effect of CO_2 on the petrophysical properties of the rocks.

The calculated values of CO_2 solubility allow for a rough estimation of the storage capacity of aquifer in order to evaluate its feasibility for geological CO_2 storage. With respect to brines with high mineralization (i.e., PL1 and LP1), CO_2 solubility is the lowest due to salting out by dissolved electrolytes. CO_2 solubility increases with increasing pressure. The impact of the temperature is not explicit because the increase in temperature decreases the Henry's law constant ($K_{H\ at\ 298K} = 10^{-1.47}$, $K_{H\ at\ 413K} = 10^{-2.06}$) [60], but at the same time the fugacity coefficient at a given pressure increases. The impact of pressure and temperature on CO_2 solubility in PL1 brine is presented in Figure 6. For reservoir brines, the solubility of CO_2 and CH_4 under reservoir conditions was calculated (see Table 5).

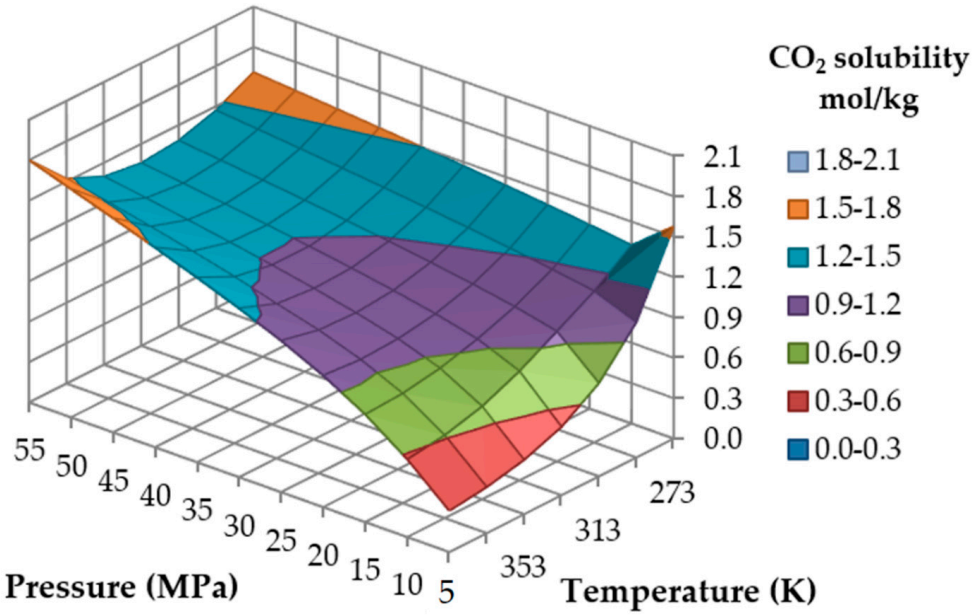

Figure 6. Calculated CO_2 solubility (mol/kg water) in PL1 brine.

Table 5. Calculated CO_2 and CH_4 solubility in reservoir brines at given initial conditions.

Reservoir	PL1	LP1	LP2	SP1	SP2
CO_2 solubility (mol/kg brine)	1.792	1.283	1.219	1.366	1.365
CH_4 solubility (mol/kg brine)	0.421	0.083	0.102	0.208	0.198

The calculations show that CO_2 dissolves 10 times better in the reservoir brine when compared to the methane solubility. Bearing the above in mind, at favorable conditions native natural gas may be displaced during CO_2 injection from aquifers. Displaced/released methane will therefore migrate from the brine and supplement the resources of the existing reservoirs.

4. Conclusions

The investigated reservoir fluids, both brines and oils, have chemical compositions and properties that favor CO_2 injection. The oils from the PL1, LP1, LP2, SP1 and SP2 oil fields belong to the group of medium paraffin-based crude oils with low asphaltene content. The MMP values are relatively low (approx. 8.3 MPa at 313 K), which assures miscible CO_2 flooding under reservoir conditions. The SRK EoS is an effective tool in analyzing the miscibility of the CO_2–oil systems. The proposed simplified approach to simulate oil composition and calculate the MMP value demonstrates a good agreement

with the experimental values. The maximum relative errors for this calculation algorithm were found to be 2.01% and 7.72% for the CO_2–*n*-decane and CO_2–LP2 systems, respectively. The CO_2 MMP depends on the reservoir temperature, oil composition and the presence of C1–C2 components. The MMP increases with the increasing reservoir temperature. At the lowest reservoir temperature of 299 K, the MMP for LP1 oil is 6.29 MPa, while for PL1 oil at 392 K the MMP is equal to 18.1 MPa. For all considered reservoirs the miscible CO_2 flooding may be achieved as the calculated MMPs at reservoir temperatures are lower than the initial reservoir pressures. In general, the presence of CH_4 dissolved in oil increases the CO_2 MMP. When the GOR changes from 10 to 100 m^3/m^3 the MMP increases from 8.40 to 8.85 MPa. The crude oil composition has a moderate effect on the MMP.

The oil field brines studied in this work show various mineralization degrees. In terms of storage capacity, reservoir waters from the SP1 and SP2 oil fields are the most promising because their CO_2 solubility is estimated to equal ca. 1.36 mol/kg of brine. The knowledge about the mutual interactions between CO_2–brine and CO_2–oil is essential when planning injection scenarios and monitoring the storage integrity.

Author Contributions: Conceptualization, E.K.; methodology, E.K. and K.C.-L.; software, E.K. and K.C.-L.; validation, E.K. and K.C.-L.; formal analysis, E.K. and K.C.-L.; investigation, E.K. and K.C.-L.; resources, E.K.; data curation, E.K.; writing—original draft preparation, E.K.; writing—review and editing, E.K. and K.C.-L.; visualization, E.K.; supervision, E.K.; project administration, E.K.; funding acquisition, E.K. All authors have read and agreed to the published version of the manuscript.

Funding: The research leading to these results has received partial funding from the Polish–Norwegian Research Programme operated by the National Centre for Research and Development under the Norwegian Financial Mechanism 2009–2014 in the frame of Project Contract No Pol-Nor/235294/99/2014

Conflicts of Interest: The authors declare no conflict of interest.

Appendix A

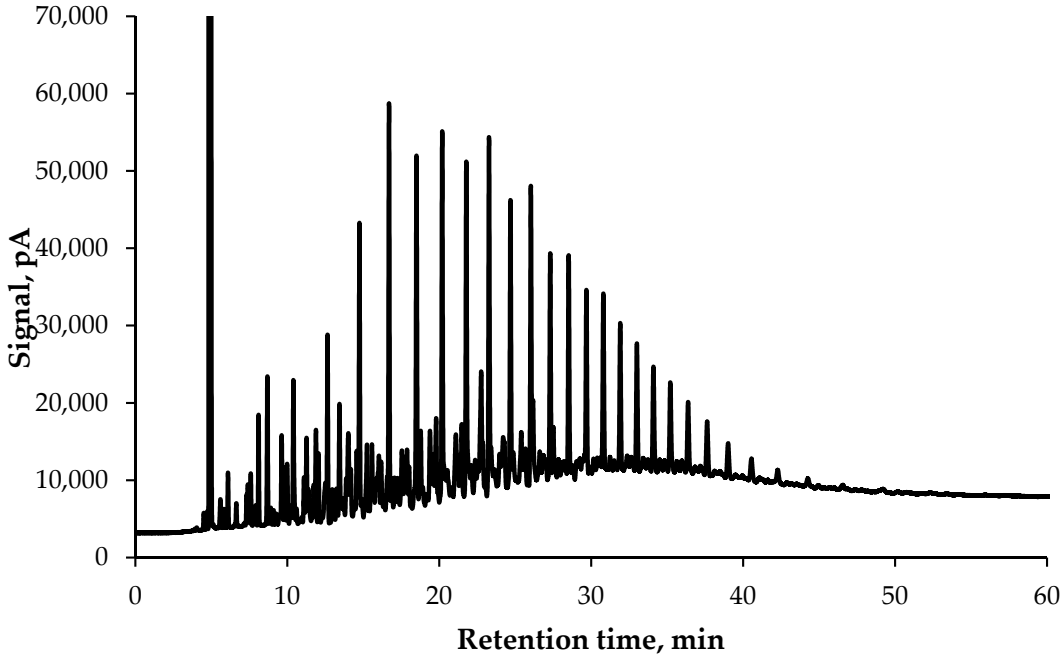

Figure A1. Whole oil LP1 gas chromatogram.

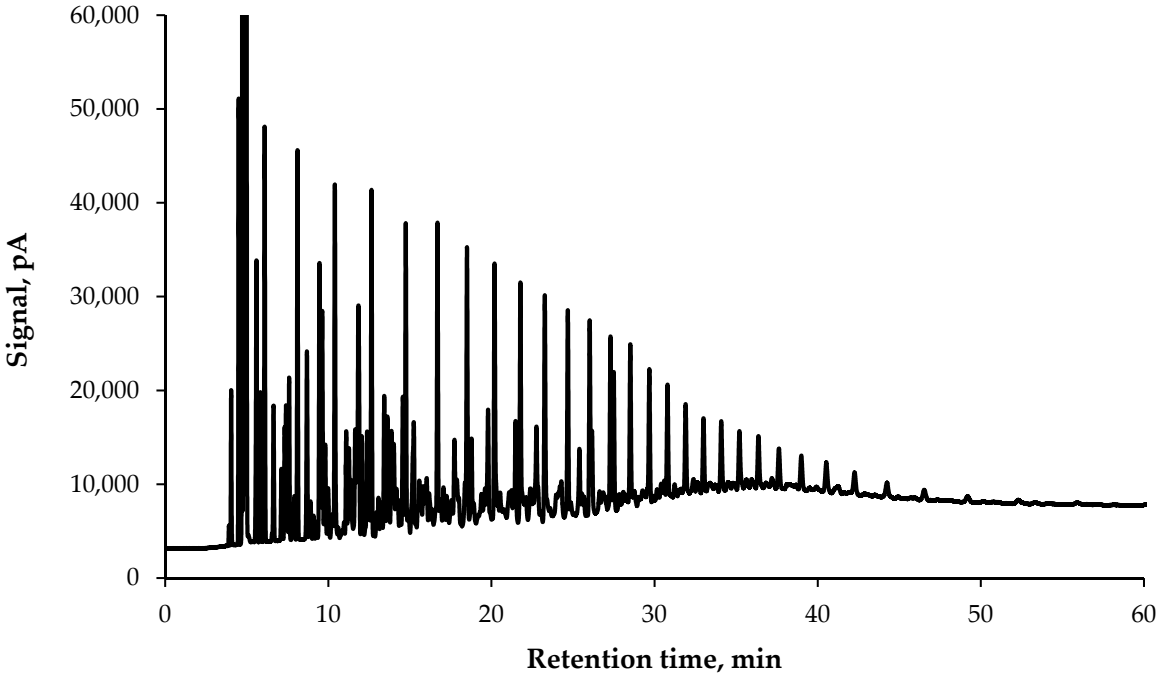

Figure A2. Whole oil PL1 gas chromatogram.

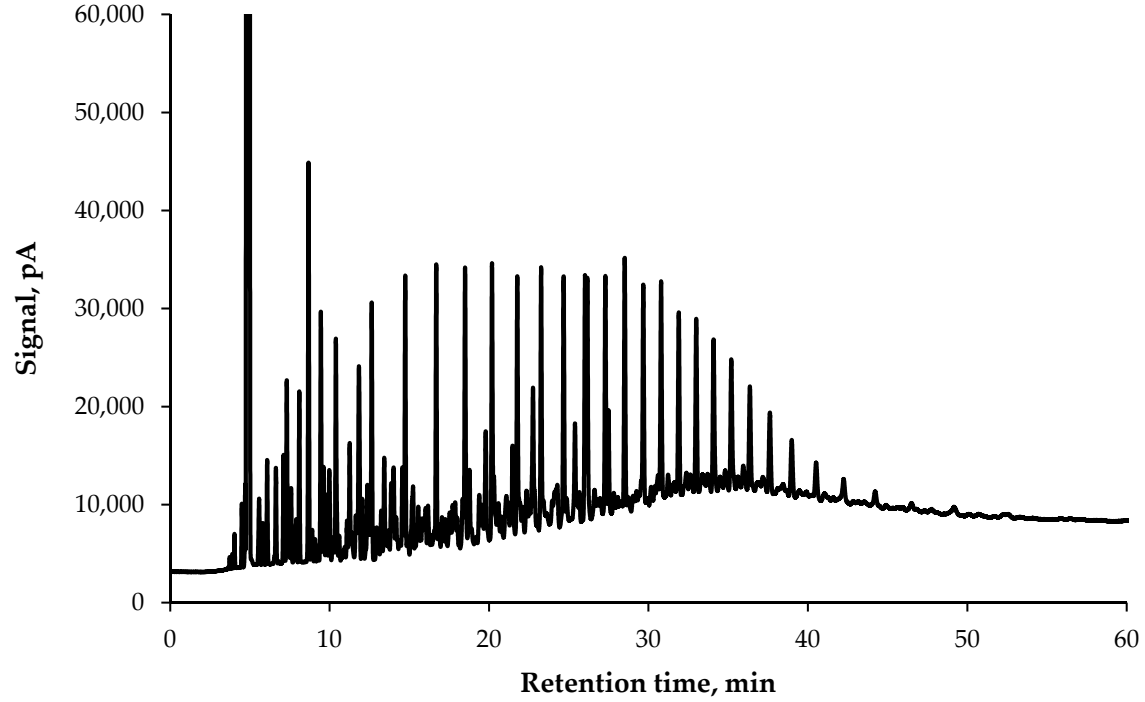

Figure A3. Whole oil SP2 gas chromatogram.

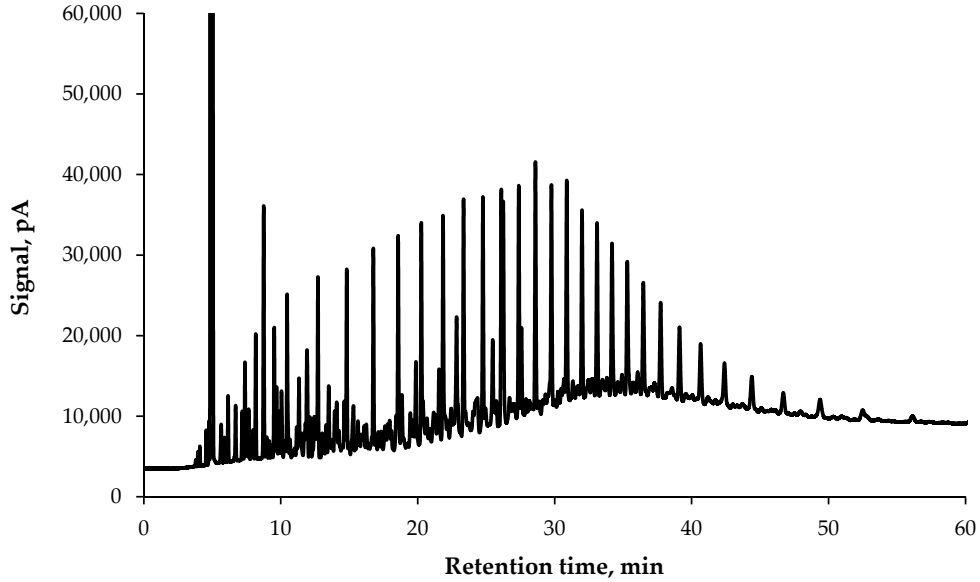

Figure A4. Whole oil SP1 gas chromatogram.

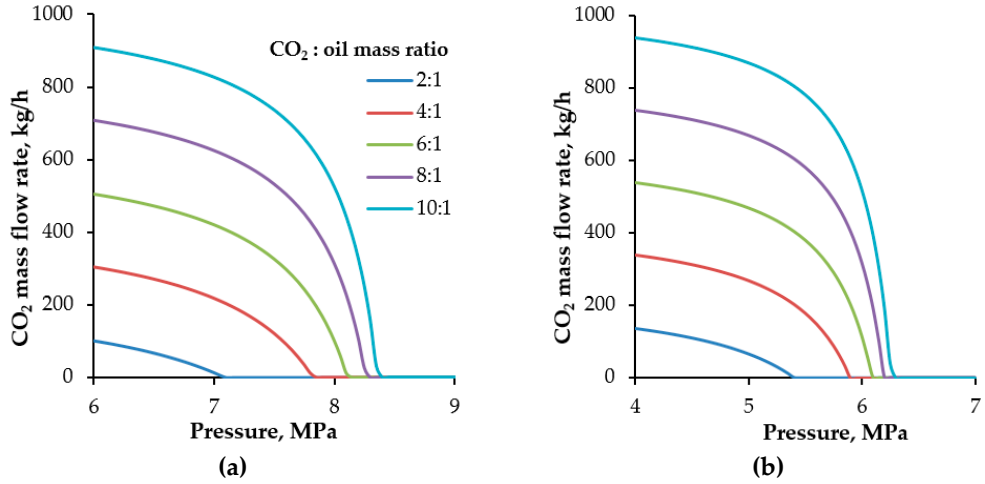

Figure A5. Graphical determination of the MMP for CO_2–LP1 oil at (**a**) 313 K, (**b**) 299 K.

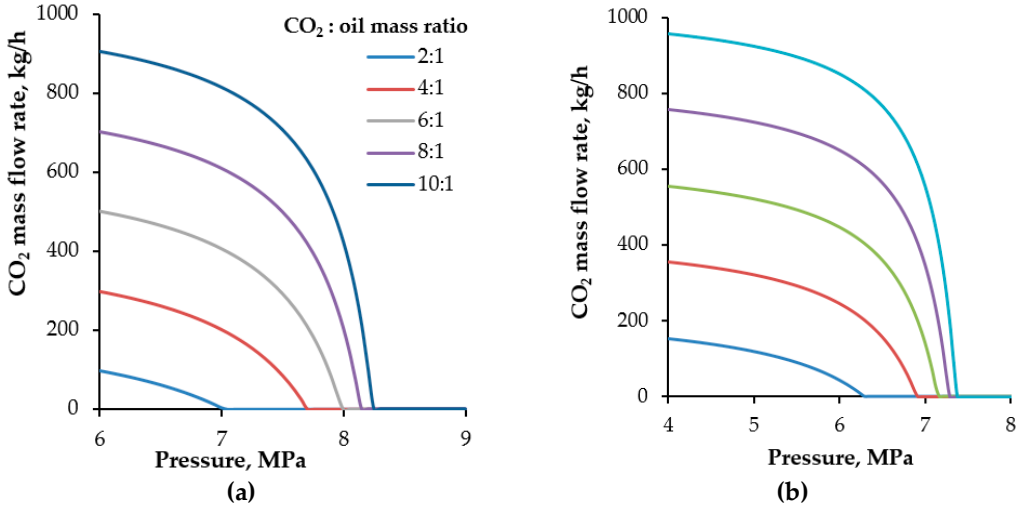

Figure A6. Graphical determination of CO_2–LP2 oil at (**a**) 313 K, (**b**) 307 K.

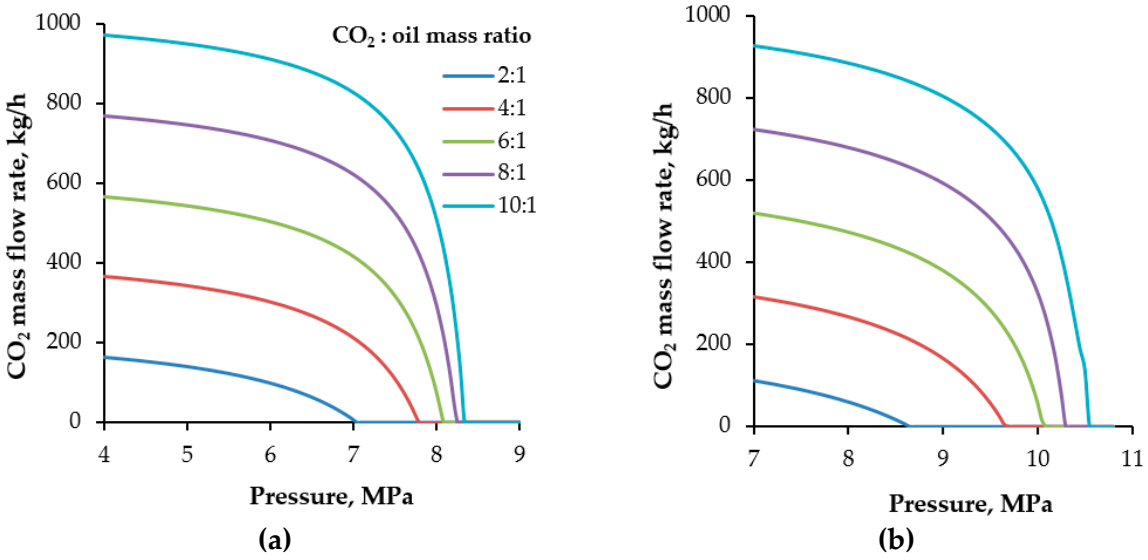

Figure A7. Graphical determination of CO_2–SP2 oil at (**a**) 313 K, (**b**) 325 K.

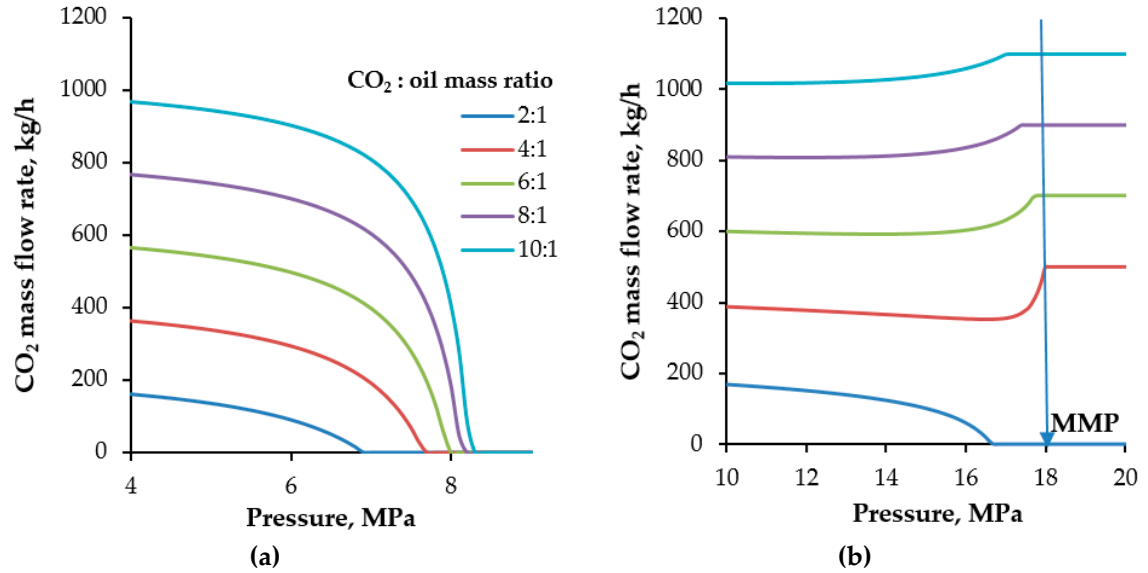

Figure A8. Graphical determination of CO_2–PL1 oil at (**a**) 313 K, (**b**) 392 K.

At higher temperatures, the mixture composed of 1000 kg of CO_2 and 100 kg of PL1 oil has a critical point at 358.9 K and 14.64 MPa. For each CO_2/oil proportion, these critical parameters slightly shift. Generally, at 392 K, which is the reservoir temperature for PL1 oil, the PL1 oil and CO_2 form a supercritical fluid. In the CHEMCAD simulator a binary mixture forms a single gaseous phase if the critical point of the mixture is exceeded. The software denotes the supercritical state with a vapor fraction equal to 1 (as gas phase). As such, in Figure A8 the mass flow rate is not going to be the zero value. It rises with the pressure until the full miscibility is achieved, and all components form a supercritical fluid. In this case the MMP value is determined as shown in Figure A8. A similar situation is observed for SP1 oil.

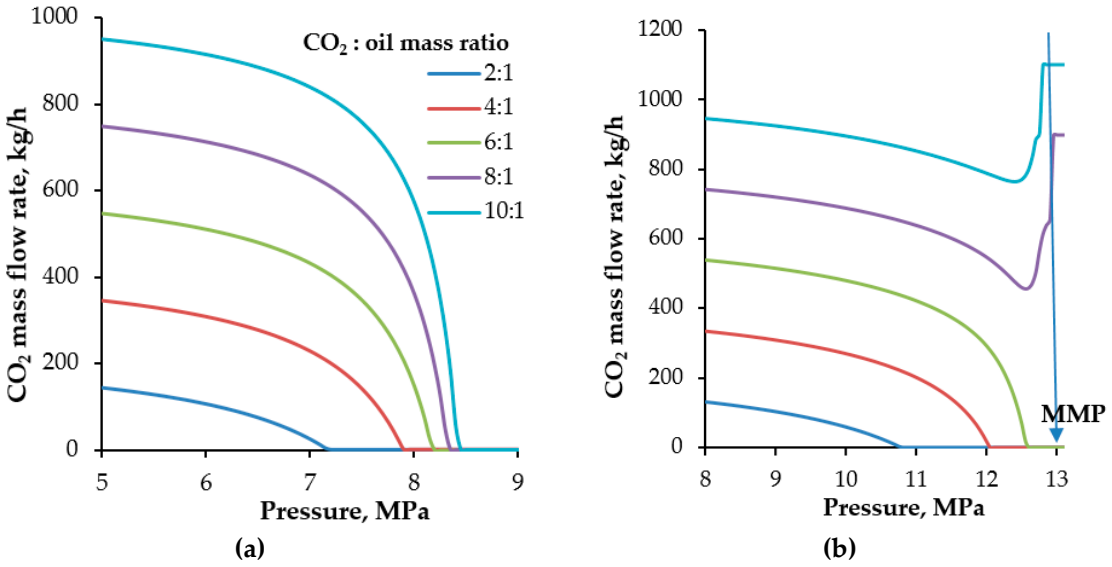

Figure A9. Graphical determination of the MMP for CO_2–SP1 oil at (**a**) 313 K, (**b**) 338 K.

References

1. General Secretariat of the Council. Conclusions on 2030 Climate and Energy Policy Framework. Note, European Commission (EC), Brussels; October 2014. Available online: http://ec.europa.eu/clima/policies/2030/documentation_en.%0Ahtm (accessed on 22 October 2019).
2. Communication from the Commission to the European Parliament, the European Council, the Council, the European Econnomic and Social Committee and the Committee of the Regions. The European Green Deal. COM/2019/640 Final. Available online: https://eur-lex.europa.eu/resource.html?uri=cellar:b828d165-1c22-11ea-8c1f-01aa75ed71a1.0002.02/DOC_1&format=PDF (accessed on 22 September 2020).
3. Wang, M.; Joel, A.S.; Ramshaw, C.; Eimer, D.; Musa, N.M. Process intensification for post-combustion CO_2 capture with chemical absorption: A critical review. *Appl. Energy* **2015**, *158*, 275–291. [CrossRef]
4. Czarnota, R.; Knapik, E.; Wojnarowski, P.; Janiga, D.; Stopa, J. Carbon dioxide separation technologies. *Arch. Min. Sci.* **2019**, *64*, 487–498.
5. Wang, M.; Lawal, A.; Stephenson, P.; Sidders, J.; Ramshaw, C. Post-combustion CO_2 capture with chemical absorption: A state-of-the-art review. *Chem. Eng. Res. Des.* **2011**, *89*, 1609–1624. [CrossRef]
6. Yildirim, O.; Kiss, A.A.; Hüser, N.; Leßmann, K.; Kenig, E.Y. Reactive absorption in chemical process industry: A review on current activities. *Chem. Eng. J.* **2012**, *213*, 371–391. [CrossRef]
7. Karayannis, V.; Charalampides, G.; Lakioti, E. Socio-economic aspects of CCS technologies. *Procedia Econ. Financ.* **2014**, *14*, 295–302. [CrossRef]
8. Venkatraman, A.; Lake, L.W.; Johns, R.T. Modelling the impact of geochemical reactions on hydrocarbon phase behavior during CO_2 gas injection for enhanced oil recovery. *Fluid Phase Equilib.* **2015**, *402*, 56–68. [CrossRef]
9. Yadala, S.; Cremaschi, S. Design and optimization of artificial cultivation units for algae production. *Energy* **2014**, *78*, 23–39. [CrossRef]
10. Zhang, C.; Jun, K.-W.; Kwak, G.; Lee, Y.-J.; Park, H.-G. Efficient utilization of carbon dioxide in a gas-to-methanol process composed of CO_2/steam–mixed reforming and methanol synthesis. *J. CO_2 Util.* **2016**, *16*, 1–7. [CrossRef]
11. Ackiewicz, M.; Foster, C.; Bonijoly, D.; Ramsak, P.; Al-Eidan, A.; Surridge, T. *CO_2 Utilisation Options—Phase 1 Report*; Technical group report; Carbon Sequestration Leadership Forum (CSLF): Washington, DC, USA, 2012.
12. Kurz, B.A.; Sorensen, J.A.; Hawthorne, S.B.; Smith, S.A.; Sanei, H.; Ordakani, O.; Walls, J.; Jin, L.; Butler, S.K.; Beddoe, J.C.; et al. The influence of organics on supercritical CO_2 migration in organic- rich shales. In Proceedings of the Unconventional Resources Technology Conference, Houston, TX, USA, 23–25 July 2018.

13. Gamadi, T.D.; Sheng, J.J.; Soliman, M.Y.; Menouar, H.; Watson, M.C.; Emadibaladehi, H. An experimental study of cyclic CO_2 injection to improve shale oil recovery. In Proceedings of the SPE Improved Oil Recovery Symposium, Tulsa, OK, USA, 12–16 April 2014.
14. Song, C.; Yang, D. Experimental and numerical evaluation of CO_2 huff-n-puff processes in Bakken formation. *Fuel* **2017**, *190*, 145–162. [CrossRef]
15. Du, F.; Nojabaei, B. A review of gas injection in shale reservoirs: Enhanced oil/gas recovery approaches and greenhouse gas control. *Energies* **2019**, *12*, 2355. [CrossRef]
16. Jia, B.; Tsau, J.-S.; Barati, R. A review of the current progress of CO_2 injection EOR and carbon storage in shale oil reservoirs. *Fuel* **2019**, *236*, 404–427. [CrossRef]
17. Uliasz-Misiak, B.; Przybycin, A. The perspectives and barriers for the implementation of CCS in Poland. *Greenh. Gases Sci. Technol.* **2016**, *6*, 7–18. [CrossRef]
18. Institute of the Environmental Protection-National Research Institute. *The National Centre for Emissions Management. Krajowy Raport Inwentaryzacyjny 2019. Inwentaryzacja Gazów Cieplarnianych dla lat 1988–2017*; Institute of the Environmental Protection-National Research Institute: Warsaw, Poland, 2019.
19. Gutmann, K.; Huscher, J.; Urbaniak, D.; White, A.; Schaible, C.; Bricke, M. Europe's Dirty 30 How the EU's Coal-Fired Power Plants Are Undermining Its Climate Efforts Highlights. 2014. Available online: http://awsassets.panda.org/downloads/dirty_30_report_finale.pdf (accessed on 12 February 2016).
20. Więcław-Solny, L.; Tatarczuk, A.; Stec, M.; Krótki, A. Advanced CO_2 capture pilot plant at tauron's coal-fired power plant: Initial results and further opportunities. *Energy Procedia* **2014**, *63*, 6318–6322. [CrossRef]
21. Stec, M.; Tatarczuk, A.; Wiecław-Solny, L.; Krótki, A.; Spietz, T.; Wilk, A.; Śpiewak, D. Demonstration of a post-combustion carbon capture pilot plant using amine-based solvents at the Łaziska Power Plant in Poland. *Clean Technol. Environ. Policy* **2016**, *18*, 151–160. [CrossRef]
22. Wolf, K.H.A.A.; van Bergen, F.; Ephraim, R.; Pagnier, H. Determination of the cleat angle distribution of the RECOPOL coal seams, using CT-scans and image analysis on drilling cuttings and coal blocks. *Int. J. Coal Geol.* **2008**, *73*, 259–272. [CrossRef]
23. Lubaś, J. Pionierskie doswiadczenia Polski w zakresie sekwestracji dwutlenku wegla. *Prz. Geol.* **2007**, *55*, 663–665.
24. Kern, F.; Gaede, J.; Meadowcroft, J.; Watson, J. The political economy of carbon capture and storage: An analysis of two demonstration projects. *Technol. Forecast. Soc. Chang.* **2016**, *102*, 250–260. [CrossRef]
25. Eccles, J.K.; Pratson, L. A "carbonshed" assessment of small-vs. large-scale CCS deployment in the continental US. *Appl. Energy* **2014**, *113*, 352–361. [CrossRef]
26. Tarkowski, R.; Misiak, B.U.; Wójcicki, A. CO_2 storage capacity of deep aquifers and hydrocarbon fields in Poland-EU GeoCapacity. Project results. *Energy Procedia* **2009**, *1*, 2671–2677.
27. Wojnarowski, P. Analiza mozliwosci zwiekszenia efektywnosci wydobycia ropy naftowej z Polskich złóż w oparciu metody EOR. *Miner. Resour. Manag.* **2012**, *28*, 47–58.
28. Mikołajczak, E.; Kosowski, P.; Stopa, J.; Wartak, J. Analysis and selection of CO_2 sources for CCS-EOR projects in oil fields clusters in Poland. *AGH Drill. Oil Gas* **2018**, *35*, 295–306. [CrossRef]
29. Kharaka, Y.K.; Maest, A.S.; Carothers, W.W.; Law, L.M.; Lamothe, P.J.; Fries, T.L. Geochemistry of metal-rich brines from central Mississippi Salt Dome basin, USA. *Appl. Geochem.* **1987**, *2*, 543–561. [CrossRef]
30. Eaton, A. (Ed.) *Standard Methods for the Examination of Water and Wastewater*, 21st ed.; APHA-AWWA-WEF: Washington, DC, USA, 2005.
31. Gonzalez, A.; Coquelet, C.; Paricaud, P.; Chapoy, A. Comparative study of vapour-liquid equilibrium and density modelling of mixtures related to carbon capture and storage with the SRK, PR, PC-SAFT and SAFT-VR Mie equations of state for industrial uses. *Fluid Phase Equilib.* **2017**, *440*, 19–35.
32. Valderrama, J.O.; Silva, A. Modified Soave-Redlich-Kwong equations of state applied to mixtures containing supercritical carbon dioxide. *Korean J. Chem. Eng.* **2003**, *20*, 709–715. [CrossRef]
33. Karim, A.M.A.; Abdel-Rahman, Z.A.; Hadi, A. Solubility prediction of CO_2 in several physical liquid solvents using Chemcad and Hysys simulators. *Dilaya J. Eng. Sci.* **2010**, *3*, 356–373.
34. Akberov, R.R. Calculating the vapor—Liquid phase equilibrium for multicomponent systems using the Soave-Redlich-Kwong equation. *Theor. Found. Chem. Eng.* **2011**, *45*, 312–318. [CrossRef]

35. Choubineh, A.; Helalizadeh, A.; Wood, D.A. The impacts of gas impurities on the minimum miscibility pressure of injected CO_2-rich gas—Crude oil systems and enhanced oil recovery potential. *Pet. Sci.* **2019**, *16*, 117–126. [CrossRef]
36. Bethke, C.M. *Geochemical Reaction Modeling: Concepts and Applications*; Oxford University Press: Oxford, UK, 1996; pp. 110–150.
37. Perez-Villasenor, F.; Iglesias-Silva, G.A. Osmotic and activity coefficients using a modified Pitzer equation for strong electrolytes 1:1 and 1:2 at 298.15 K. *Ind. Eng. Chem. Res.* **2002**, *41*, 1031–1037. [CrossRef]
38. Ayirala, S.C.; Xu, W.; Rao, D.N. Interfacial behaviour of complex hydrocarbon fluids at elevated pressures andtemperatures. *Can. J. Chem. Eng.* **2006**, *84*, 22–32. [CrossRef]
39. Asghari, K.; Torabi, F. Effect of miscible and immiscible CO_2 injection on gravity drainage: Experimental and simulation results. In Proceedings of the SPE Symposium on Improved Oil Recovery, Tulsa, OK, USA, 20–23 April 2008.
40. Song, Y.-C.; Zhu, N.J.; Yu, L.; Zhao, J.-F.; Liu, W.-G.; Zhang, Y.; Zhao, Y.-C.; Jiang, L.-L. Magnetic resonance imaging study on the miscibility of a CO_2/n-decane. *Chin. Phys. Lett.* **2011**, *28*, 096401. [CrossRef]
41. Liu, Y.; Jiang, L.; Tang, L.; Song, Y.; Zhao, J.; Zhang, Y.; Wang, D.; Yang, M. Minimum miscibility pressure estimation for a CO_2/n-decane system in porous media by X-ray CT. *Exp. Fluids* **2015**, *56*, 7. [CrossRef]
42. Elsharkawy, A.; Poettmann, F.; Christiansen, R. Measuring CO_2 minimum miscibility pressures: Slim-tube or rising-bubble method? *Energy Fuels* **1996**, *10*, 443–449. [CrossRef]
43. Czarnota, R.; Janiga, D.; Stopa, J.; Wojnarowski, P. Determination of minimum miscibility pressure for CO_2 and oil system using acoustically monitored separator. *J. CO2 Util.* **2017**, *17*, 32–36. [CrossRef]
44. Zhang, P.Y.; Huang, S.; Sayegh, S.; Zhou, X.L. Effect of CO_2 impurities on gas-injection EOR processes. In Proceedings of the SPE/DOE Symposium on Improved Oil Recovery, Tulsa, OK, USA, 17–21 April 2004.
45. Karnkowski, P. *Oil and Gas Deposits in Poland*; Geosynoptics Society GEOS: Cracow, Poland, 1999.
46. Dong, M.; Huang, S.; Srivastava, R. Effect of solution gas in oil on CO_2 minimum miscibility pressure. *J. Can. Pet. Technol.* **2000**, *11*, 53–61.
47. Alston, R.B.; Kokolis, G.P.; James, C.F. CO_2 minimum miscibility pressure: A correlation for impure CO_2 streams and live oil systems. *Soc. Pet. Eng. J.* **1985**, *25*, 268–274. [CrossRef]
48. Jia, B.; Tsau, J.-S.; Barati, R. Role of molecular diffusion in heterogeneous, naturally fractured shale reservoirs during CO_2 huff-n-puff. *J. Pet. Sci. Eng.* **2018**, *164*, 31–42. [CrossRef]
49. Jia, B.; Tsau, J.-S.; Barati, R. Measurement of CO_2 diffusion coefficient in the oil-saturated porous media. *J. Pet. Sci. Eng.* **2019**, *181*, 106189. [CrossRef]
50. Zhou, X.; Jiang, Q.; Yuan, Q.; Zhang, L.; Feng, J.; Chu, B.; Zeng, F.; Zhu, G. Determining CO_2 diffusion coefficient in heavy oil in bulk phase and in porous media using experimental and mathematical modeling methods. *Fuel* **2020**, *263*, 116205. [CrossRef]
51. Wang, S.; Ma, M.; Chen, S. Application of PC-SAFT equation of state for CO_2 minimum miscibility pressure prediction in nanopores. In Proceedings of the SPE Improved Oil Recovery Conference, Tulsa, OK, USA, 11–13 April 2006.
52. McLing, T.; Smith, W.; Smith, R. Utilizing rare earth elements as tracers in high TDS reservoir brines in CCS applications. *Energy Procedia* **2014**, *63*, 3963–3974. [CrossRef]
53. Rohmer, J.; Pluymakers, A.; Renard, F. Mechano-chemical interactions in sedimentary rocks in the context of CO_2 storage: Weak acid, weak effects? *Earth Sci. Rev.* **2016**, *157*, 86–110. [CrossRef]
54. Kim, S.; Santamarina, J.C. Geometry-coupled reactive fluid transport at the fracture scale: Application to CO_2 geologic storage. *Geofluids* **2016**, *16*, 329–341. [CrossRef]
55. Gaus, I. Role and impact of CO_2-rock interactions during CO_2 storage in sedimentary rocks. *Int. J. Greenh. Gas Control* **2010**, *4*, 73–89. [CrossRef]
56. Adamczyk, K.; Schwarz-Premont, M.; Pines, D.; Pines, E.; Nibbering, E. Real-time observation of carbonic acid formation in aqueous solution. *Science* **2009**, *326*, 1690–1694. [CrossRef] [PubMed]
57. Gaus, I.; Audigane, P.; Andre, L.; Lions, J.; Jacquemet, N.; Durst, P.; Czernichowski-Lauriol, I.; Azaroual, M. Geochemical and solute transport modelling for CO_2 storage, what to expect from it? *Int. J. Greenh. Gas Control* **2008**, *2*, 605–625. [CrossRef]
58. Rimmelé, G.; Barlet-Gouédard, V.; Renard, F. Evolution of the petrophysical and mineralogical properties of two reservoir rocks under thermodynamic conditions relevant for CO_2 geological storage at 3 km depth. *Oil Gas Sci. Technol.* **2010**, *65*, 565–580. [CrossRef]

59. Hangx, S.J.T.; Pluymakers, A.M.H.; Ten Hove, A.; Spiers, C.J. The effects of lateral variations in rock composition and texture on anhydrite caprock integrity of CO_2 storage systems. *Int. J. Rock Mech. Min. Sci.* **2014**, *69*, 80–92. [CrossRef]
60. Gilbert, K.; Bennett, P.C.; Wolfe, W.; Zhang, T.; Romanak, K.D. CO_2 solubility in aqueous solutions containing Na^+, Ca^{2+}, Cl^-, $SO_4{}^{2-}$ and $HCO_3{}^-$: The effects of electrostricted water and ion hydration thermodynamics. *Appl. Geochem.* **2016**, *67*, 59–67. [CrossRef]